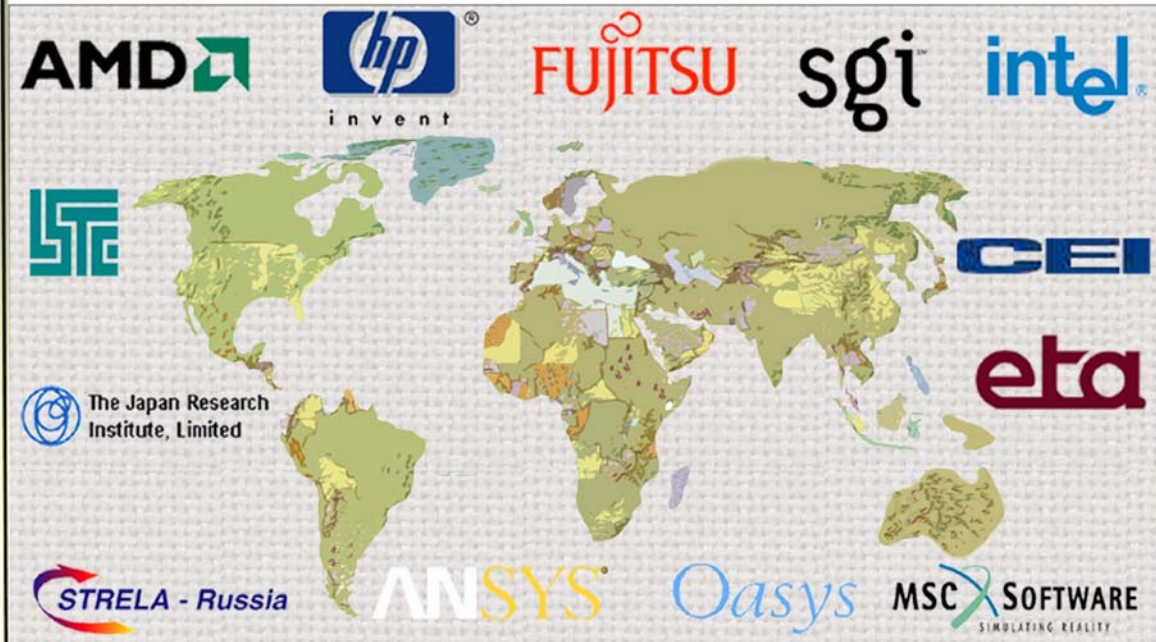


February 2003

Worldwide News



FEA Information Inc.

LEAP -Australia

**ALTAIR - Western Region
US**

DYNAMAX - US

**Cril Technology
Simulation - France**

GISSETA - India

MFAC -Canada

DYNAmore - Germany

**FLOTREND -
Taiwan**

KOSTECH - Korea

ERAB - Sweden

THEME - Korea

ALTAIR - Italy

CAD-FEM -Germany

Numerica SRL - Italy

Dr. Ted Belytschko - US

**Prof Gennaro
Monacelli - Italy**

Dr. Bhavin V. Mehta - US

Dr. Taylan Altan - US

Dr. David Benson - US

**Dr. Alexey I.
Borovkov - Russia**

Prof. Ala Tabiei - US



FEA Information Inc. Worldwide News

February - Volume 4

Issue 02-2003

01	LSTC Optimization Methodology – LS-OPT 2.1 through 2.5.4
08	4 th European LS-DYNA Conference list of submitted papers
13	FEA January Site Information
14	FEA Information Participants
15	FEA Information Events Page Listings
16	Zero Energy Modes in One Dimension: An Introduction to “Hourglass” Modes – David J. Benson

Editor	Trent Eggleston
Editor Technical Content	Arthur B. Shapiro
Technical Writer	David Benson
Technical Writer	Uli Franz
Graphic Designer	Wayne Mindle
Feature Director	Marsha Victory

The contents of this publication is deemed to be accurate and complete. However, FEA Information Inc. doesn't guarantee or warrant accuracy or completeness of the material contained herein. All trademarks are the property of their respective owners. This publication is published for FEA Information Inc., Copyright 2002. All rights reserved. Not to be reproduced in hardcopy or electronic format.

Announcement: New Participant

numerica

Italian LS-DYNA distributor

VPS - Virtual Paint Shop

Numerica Srl Via Panciatichi, 40 Firenze

Ph +39.055.432010 www.numerica-srl.it

2.1 Introduction

In the conventional design approach, a design is improved by evaluating its response and making design changes based on experience or intuition. This approach does not always lead to the desired result, that of a 'best' design, since design objectives are sometimes in conflict, and it is not always clear how to change the design to achieve the best compromise of these objectives. A more systematic approach can be obtained by using an inverse process of first specifying the criteria and then computing the 'best' design. The procedure by which design criteria are incorporated as objectives and constraints into an optimization problem that is then solved, is referred to as optimal design.

The state of computational methods and computer hardware has only recently advanced to the level where complex nonlinear problems can be analyzed routinely. Many examples can be found in the simulation of impact problems and manufacturing processes. The responses resulting from these time-dependent processes are, as a result of behavioral instability, often highly sensitive to design changes. Program logic, as for instance encountered in parallel programming or adaptivity, may cause spurious sensitivity. Roundoff error may further aggravate these effects, which, if not properly addressed in an optimization method, could obstruct the improvement of the design by way of corrupting the function gradients.

Among several methodologies available to address optimization in this design environment, *response surface methodology (RSM)*, a statistical method for constructing smooth approximations to functions in a multi-dimensional space, has achieved prominence in recent years. Rather than relying on local information such as a gradient only, RSM selects designs that are optimally distributed throughout the design space to construct approximate surfaces or 'design formulae'. Thus, the local effect caused by 'noise' is alleviated and the method attempts to find a representation of the design response within a bounded design space or smaller region of interest. This extraction of global information allows the designer to explore the design space, using alternative design formulations. For instance, in vehicle design, the designer may decide to investigate the effect of varying a mass constraint, while monitoring the crashworthiness responses of a vehicle. The designer might also decide to constrain the crashworthiness response while minimizing or maximizing any other criteria such as mass, ride comfort criteria, etc. These criteria can be weighted differently according to importance and therefore the design space needs to be explored more widely.

Part of the challenge of developing a design program is that designers are not always able to clearly define their design problem. In some cases, design criteria may be regulated by safety or other considerations and therefore a response has to be constrained to a specific value. These can be easily defined as mathematical constraint equations. In other cases, fixed criteria are not available but the designer knows whether the responses must be minimized or maximized. In vehicle design, for instance, crashworthiness can be constrained because of regulation, while other parameters such as mass, cost and ride comfort can be treated as objectives to be weighted according to importance. In these cases, the designer may have target values in mind for the various response and/or design parameters, so that the objective formulation has to be formulated to approximate the target values as closely as possible. Because the relative importance of various criteria can be subjective, the ability to visualize the trade-off properties of one response vs. another becomes important.

Trade-off curves are visual tools used to depict compromise properties where several important response parameters are involved in the same design. They play an extremely important role in modern design where design adjustments must be made accurately and rapidly. Design trade-off curves are constructed using the principle of *Pareto* optimality. This implies that only those designs of which the improvement of one response

will necessarily result in the deterioration of any other response are represented. In this sense no further improvement of a Pareto optimal design can be made: it is the best compromise. The designer still has a choice of designs but the factor remaining is the subjective choice of which feature or criterion is more important than another. Although this choice must ultimately be made by the designer, these curves can be helpful in making such a decision. An example in vehicle design is the trade-off between mass (or energy efficiency) and safety.

Adding to the complexity, is the fact that mechanical design is really an interdisciplinary process involving a variety of modeling and analysis tools. To facilitate this process, and allow the designer to focus on creativity and refinement, it is important to provide suitable interfacing utilities to integrate these design tools. Designs are bound to become more complex due to the legislation of safety and energy efficiency as well as commercial competition. It is therefore likely that in future an increasing number of disciplines will have to be integrated into a particular design. This approach of multidisciplinary design requires the designer to run more than one case, often using more than one type of solver. For example, the design of a vehicle may require the consideration of crashworthiness, ride comfort, noise level as well as durability. Moreover, the crashworthiness analysis may require more than one analysis case, e.g. frontal and side impact. It is therefore likely that as computers become more powerful, the integration of design tools will become more commonplace, requiring a multidisciplinary design interface.

Modern architectures often feature multiple processors and all indications are that the demand for distributed computing will strengthen into the future. This is causing a revolution in computing as single analyses that took a number of days in the recent past can now be done within a few hours. Optimization, and RSM in particular, lend themselves very well to being applied in distributed computing environments because of the low level of message passing. Response surface methodology is efficiently handled, since each design can be analyzed independently during a particular iteration. Needless to say, sequential methods have a smaller advantage in distributed computing environments than global search methods such as RSM.

The present version of LS-OPT also features Monte Carlo based point selection schemes and optimization methods. The respective relevance of stochastic and response surface based methods may be of interest. In a pure response surface based method, the effect of the variables is distinguished from chance events while Monte Carlo simulation is used to investigate the effect of these chance events. The two methods should be used in a complimentary fashion rather than substituting the one for the other. In the case of events in which chance plays a significant role, responses of design interest are often of a global nature (being averaged or integrated over time). These responses are mainly deterministic in character. The full vehicle crash example in this manual can attest to the deterministic qualities of intrusion and acceleration pulses. These types of responses may be highly nonlinear and have random components due to uncontrollable noise variables, but they are not random.

Stochastic methods have also been touted as design improvement methods. In a typical approach, the user iteratively selects the best design results of successive stochastic simulations to improve the design. These design methods, being dependent on chance, are generally not as efficient as response surface methods. However, an iterative design improvement method based on stochastic simulation is available in LS-OPT.

Stochastic methods have an important purpose when conducted directly or on the surrogate (approximated) design response in reliability based design optimization and robustness improvement. This methodology is currently under development and will be available in future versions of LS-OPT.

Theory of Optimization

Optimization can be defined as a procedure for “achieving the best outcome of a given operation while satisfying certain restrictions” [17]. This objective has always been central to the design process, but is now

assuming greater significance than ever because of the maturity of mathematical and computational tools available for design.

Mathematical and engineering optimization literature usually presents the above phrase in a standard form as

$$\min f(\mathbf{x}) \tag{0.1}$$

subject to

$$g_j(\mathbf{x}) \leq 0 \quad ; \quad j = 1, 2, \dots, m$$

and

$$h_k(\mathbf{x}) = 0 \quad ; \quad k = 1, 2, \dots, l$$

where f , g and h are functions of independent variables $x_1, x_2, x_3, \dots, x_n$. The function f , referred to as the cost or objective function, identifies the quantity to be minimized or maximized. The functions g and h are constraint functions which represent the design restrictions. The variables collectively described by the vector \mathbf{x} are often referred to as design variables or design parameters.

The two sets of functions g_j and h_k define the constraints of the problem. The equality constraints do not appear in any further formulations presented here because algorithmically each equality constraint can be represented by two inequality constraints in which the upper and lower bounds are set to the same number, e.g.

$$h_k(\mathbf{x}) = 0 \sim 0 \leq h_k(\mathbf{x}) \leq 0 \tag{0.2}$$

Equations (2.1) then become

$$\min f(\mathbf{x}) \tag{0.3}$$

subject to

$$g_j(\mathbf{x}) \leq 0 \quad ; \quad j = 1, 2, \dots, m$$

The necessary conditions for the solution \mathbf{x}^* to Eq. (2.3) are the Karush-Kuhn-Tucker optimality conditions:

$$\begin{aligned} \nabla f(\mathbf{x}^*) + \boldsymbol{\lambda}^T \nabla \mathbf{g}(\mathbf{x}^*) &= \mathbf{0} \\ \boldsymbol{\lambda}^T \mathbf{g}(\mathbf{x}^*) &= \mathbf{0} \\ \mathbf{g}(\mathbf{x}^*) &\leq \mathbf{0} \\ \boldsymbol{\lambda} &\geq \mathbf{0}. \end{aligned} \tag{0.4}$$

These conditions are derived by differentiating the Lagrangian function of the constrained minimization problem

$$L(\mathbf{x}) = f(\mathbf{x}) + \boldsymbol{\lambda}^T \mathbf{g}(\mathbf{x}) \tag{0.5}$$

and applying the conditions

$$\nabla^T f \partial \mathbf{x}^* \geq 0 \text{ (optimality)} \tag{0.6}$$

and

$$\nabla^T \bar{\mathbf{g}} \partial \mathbf{x}^* \leq \mathbf{0} \text{ (feasibility)} \tag{0.7}$$

to a perturbation $\partial \mathbf{x}^*$.

λ_j are the Lagrange multipliers which may be nonzero only if the corresponding constraint is active, i.e. $g_j(\mathbf{x}^*) = 0$.

For x^* to be a local constrained minimum, the Hessian of the Lagrangian function, $\nabla^2 f(x^*) + \lambda^T \nabla^2 \bar{g}(x^*)$ on the subspace tangent to the active constraint \bar{g} must be positive definite at x^* .

These conditions are not used explicitly in LS-OPT and are not tested for at optima. They are more of theoretical interest in this manual, although the user should be aware that some optimization algorithms are based on these conditions.

2.2 *Gradient Computation and the Solution of Optimization Problems*

Solving the optimization problem requires an optimization algorithm. The list of optimization methods is long and the various algorithms are not discussed in any detail here. For this purpose, the reader is referred to the texts on optimization, e.g. [29] or [17]. It should however be mentioned that the Sequential Quadratic Programming method is probably the most popular algorithm for constrained optimization and is considered to be a state-of-the-art approach for structural optimization [4,53]. In LS-OPT, the subproblem is optimized by an accurate and robust gradient-based algorithm: the dynamic leap-frog method [48]. Both these algorithms and most others have in common that they are based on first order formulations, i.e. they require the first derivatives of the component functions

$$df/dx_i \text{ and } dg_j/dx_i$$

in order to construct the local approximations. These gradients can be computed either analytically or numerically. In order for gradient-based algorithms such as SQP to converge, the functions must be continuous with continuous first derivatives.

Analytical differentiation requires the formulation and implementation of derivatives with respect to the design variables in the simulation code. Because of the complexity of this task, analytical gradients (also known as design sensitivities) are mostly not readily available.

Numerical differentiation is typically based on forward difference methods that require the evaluation of n perturbed designs in addition to the current design. This is simple to implement but is expensive and hazardous because of the presence of round-off error. As a result, it is difficult to choose the size of the intervals of the design variables, without risking spurious derivatives (the interval is too small) or inaccuracy (the interval is too large). Some discussion on the topic is presented in Reference [17].

As a result, gradient-based methods are typically only used where the simulations provide smooth responses, such as linear structural analysis and certain types of nonlinear analysis.

In non-linear dynamic analysis such as the analysis of impact or metal-forming, the derivatives of the response functions are mostly severely discontinuous. This is mainly due to the presence of friction and contact. The response (and therefore the sensitivities) may also be highly nonlinear due to the chaotic nature of impact phenomena and therefore the gradients may not reveal much of the overall behavior. Furthermore, the accuracy of numerical sensitivity analysis may also be adversely affected by round-off error. Analytical sensitivity analysis for friction and contact problems is a subject of current research.

It is mainly for the above reasons that researchers have resorted to global approximation methods for smoothing the design response. The art and science of developing design approximations has been a popular theme in design optimization research for decades (for a review of the various approaches, see e.g. Reference [5] by Barthelemy). Barthelemy categorizes two main global approximation methods, namely response surface methodology [10] and neural networks [19].

In the present implementation, the gradient vectors of general composites based on mathematical expressions of the basic response surfaces are computed using numerical differentiation. A default interval of 1/1000 of the size of the design space is used in the forward difference method.

2.3 *Normalization of constraints and variables*

It is a good idea to eliminate large variations in the magnitudes of design variables and constraints by normalization.

In LS-OPT, the typical constraint is formulated as follows:

$$L_j \leq g_j(\mathbf{x}) \leq U_j \quad ; \quad j=1,2,\dots,m \quad (0.8)$$

which, when normalized becomes:

$$\frac{L_j}{g_j(\mathbf{x}_0)} \leq \frac{g_j(\mathbf{x})}{g_j(\mathbf{x}_0)} \leq \frac{U_j}{g_j(\mathbf{x}_0)} \quad ; \quad j=1,2,\dots,m \quad (0.9)$$

where \mathbf{x}_0 is the starting vector. The normalization is done internally.

The design variables have been normalized internally by scaling the design space $[\mathbf{x}_L; \mathbf{x}_U]$ to $[0;1]$, where \mathbf{x}_L is the lower and \mathbf{x}_U the upper bound. The formula

$$\xi_i = \frac{x_i - x_{iL}}{x_{iU} - x_{iL}} \quad (0.10)$$

is used to transform each variable x_i to a normalized variable, ξ_i .

When using LS-OPT to minimize maximum violations, the responses must be normalized by the user. This method is chosen to give the user the freedom in selecting the importance of different responses when e.g. performing parameter identification. Section 2.15.3 will present this application in more detail.

2.4 *Response Surface Methodology*

An authoritative text on Response Surface Methodology [34] defines the method as “a collection of statistical and mathematical techniques for developing, improving, and optimizing processes.” Although an established statistical method for several decades [9], it has only recently been actively applied to mechanical design [54]. Due to the importance of weight as a criterion and the multidisciplinary nature of aerospace design, the application of optimization and RSM to design had its early beginnings in the aerospace industry. A large body of pioneering work on RSM was conducted in this and other mechanical design areas during the eighties and nineties [22,43,54,55].

Although inherently simple, the application of response surface methods to mechanical design has been inhibited by the high cost of simulation and the large number of analyses required for many design variables. In the quest for accuracy, increased hardware capacity has been consumed by greater modeling detail and therefore optimization methods have remained largely on the periphery of the area of mechanical design. In lieu of formal

methods, designers have traditionally resorted to experience and intuition to improve designs. This is seldom effective and also manually intensive. Moreover, design objectives are often in conflict, making conventional methods difficult to apply, and therefore more analysts are formalizing their design approach by using optimization.

2.5.1 Approximating the response

Response Surface Methodology (or RSM) requires the analysis of a predetermined set of designs. A design surface is fitted to the response values using regression analysis. Least squares approximations are commonly used for this purpose. The response surfaces are then used to construct an approximate design “subproblem” which can be optimized.

The response surface method relies on the fact that the set of designs on which it is based is well chosen. Randomly chosen designs may cause an inaccurate surface to be constructed or even prevent the ability to construct a surface at all. Because simulations are often time-consuming and may take days to run, the overall efficiency of the design process relies heavily on the appropriate selection of a design set on which to base the approximations. For the purpose of determining the individual designs, the theory of experimental design (Design of Experiments or DOE) is required. Several experimental design criteria are available but one of the most popular for an arbitrarily shaped design space is the D -optimality criterion. This criterion has the flexibility of allowing any number of designs to be placed appropriately in a design space with an irregular boundary. The understanding of the D -optimality criterion requires the formulation of the least squares problem.

Consider a single response variable y dependent upon a number of variables \mathbf{x} . The exact functional relationship between these quantities is

$$y = \eta(\mathbf{x}) \quad (0.11)$$

The exact functional relationship is now approximated (e.g. polynomial approximation) as

$$\eta(\mathbf{x}) \approx f(\mathbf{x}) \quad (0.12)$$

The approximating function f is assumed to be a summation of basis functions:

$$f(\mathbf{x}) = \sum_{i=1}^L a_i \phi_i(\mathbf{x}) \quad (0.13)$$

where L is the number of basis functions ϕ_i used to approximate the model.

The constants $\mathbf{a} = [a_1, a_2, \dots, a_L]^T$ have to be determined in order to minimize the sum of the square error:

$$\sum_{p=1}^P \{ [y(\mathbf{x}_p) - f(\mathbf{x}_p)]^2 \} = \sum_{p=1}^P \left\{ \left[y(\mathbf{x}_p) - \sum_{i=1}^L a_i \phi_i(\mathbf{x}_p) \right]^2 \right\} \quad (0.14)$$

P is the number of experimental points and y is the exact functional response at the experimental points \mathbf{x}_i .

The solution to the unknown coefficients is:

$$\mathbf{a} = (\mathbf{X}^T \mathbf{X})^{-1} \mathbf{X}^T \mathbf{y} \quad (0.15)$$

where \mathbf{X} is the matrix

$$\mathbf{X} = [X_{ui}] = [\phi_i(\mathbf{x}_u)] \quad (0.16)$$

The next critical step is to choose appropriate basis functions. A popular choice is the quadratic approximation

$$\phi = [1, x_1, \dots, x_n, x_1^2, x_1x_2, \dots, x_1x_n, \dots, x_n^2]^T \quad (0.17)$$

but any suitable function can be chosen. LS-OPT allows linear, elliptical (linear and diagonal terms), interaction (linear and off-diagonal terms) and quadratic functions.

2.5.2 Factors governing the accuracy of the response surface

Several factors determine the accuracy of a response surface [34].

1. *The size of the subregion.*
For problems with smooth responses, the smaller the size of the subregion, the greater the accuracy. For the general problem, there is a minimum size at which there is no further gain in accuracy. Beyond this size, the variability in the response may become indistinguishable due to the presence of ‘noise’.
2. *The choice of the approximating function.*
Higher order functions are generally more accurate than lower order functions. Theoretically, over-fitting (the use of functions of too high complexity) may occur and result in suboptimal accuracy, but there is no evidence that this is significant for polynomials up to second order [34].
3. *The number and distribution of the design points.*
For smooth problems, the prediction accuracy of the response surface improves as the number of points is increased. However, this is only true up to roughly 50% oversampling [34] (very roughly).

2.5.3 Advantages of the method

- *Design exploration*
As design is a process, often requiring feedback and design modifications, designers are mostly interested in suitable design formulae, rather than a specific design. If this can be achieved, and the proper design parameters have been used, the design remains flexible and changes can still be made at a late stage before verification of the final design. This also allows multidisciplinary design to proceed with a smaller risk of having to repeat simulations. As designers are moving towards computational prototyping, and as parallel computers or network computing are becoming more commonplace, the paradigm of design exploration is becoming more important. Response surface methods can thus be used for global exploration in a parallel computational setting. For instance, interactive trade-off studies can be conducted.
- *Global optimization*
Response surfaces have a tendency to capture globally optimal regions because of their smoothness and global approximation properties. Local minima caused by noisy response are thus avoided.

2.5.4 Other types of response surfaces

Neural network approximations can also be used as response surfaces and are discussed in section 2.13.

4th European LS-DYNA Conference
May 2003 to be held in Ulm, Germany
Submitted Papers

REDUCED CONFERENCE FEE: Early registration before 28th February 2003

Crash- / Automotive Applications

CAE Simulations onto Passive Safety focused on the Porsche Cayenne - the Transition to New Technologies

Schelkle E., Klamsner H., Dr. Ing. h. c. F. Porsche AG

How to Develop a Five Star Car by using LS-DYNA

Malcusson R., Saab Automobile AB

Consideration of Manufacturing Effects to Improve Crash Simulation Accuracy

Böttcher C.-S., Frik S., Adam Opel AG

The Development of the new XJ Jaguar in Advanced Aluminium; Opportunities and Challenges

Zeguar T., Jaguar Cars Ltd.

The Evaluation of Crashworthiness of Vehicles with Forming Effects

Kim H., KIA Motors; Hong S., Korea Advanced Institute of Science and Techn.

Safety Analysis of the New ACTROS Cabins According to ECE-R29/02

Raich H., DaimlerChrysler AG

Integration of Simulation in the development Process

Brockmann J., Faurecia GmbH & Co. KG

Strength Analysis of Seat Belt Anchorage According to ECE R14 and FMVSS 210

Hessenberger K., DaimlerChrysler AG

Validation of New Train Railway Rolling Stock using Finite Element Analysis

Ricketts B., Bombardier Transportation UK Ltd.

Impact Performance of Flexible Guardrail Systems using LS-DYNA

Sennah K., Samaan M., Elmarakbi A., Univ. of Toronto

Forming to Crash Simulation in Full Vehicle Models

Cafolla J., Hall R.W., Norman D.P., McGregor I.J., Corus Automotive Engineering

Improving the Roadside Safety with Computational Simulations

Vesenjak M., Ren Z., University of Maribor

Development of an Energy Absorbing Concept for Automotive Applications using Dynamic Simulation Method

Owens P., Cellbond Ltd.

Reasons for Scatter in Crash Simulation results

Thole C.-A., Ligan M., FhG-SCAI

Using Modal Representation, Mesh Coarsing Approaches to Reduce the CPU Demand for VPG Applications

Nasser T., eta Engineering Technology Associates

Tire Modeling

Oshita F., Japan Research Institute

Development and Applications of Modal Presentation

Tang A., eta Engineering Technology Associates

Pedestrian and Occupant Safety / Airbag Modelling

Development and Validation of Numerical Pedestrian Impactor Models

Frank Th., DaimlerChrysler AG; Kurz A., LASSO GmbH; Pitzer M., PENG GmbH; Söllner M., Dr. Ing. h. c. F. Porsche AG

Numerical and Experimental Study on Fracture of Chute Structure at Deployment of Invisible Passenger Side Airbag

Kangwook L., Hyundai Mobiles

Finite Element Models for European Testing, a Side Impact Barrier to WG-13 and Pedestrian Impactors WG17

Dutton T., ARUP

Prediction of Occupant Injury in an Out-Of-Position Impact Using the Fluid Structure Interaction Capabilities in LS-DYNA

Marklund P.-O., Engineering Research Nordic AB; Pipkorn B., Autoliv Research AB

***MAT_GAS_MIXTURE, A New Gas Mixture Model for Airbag Applications**

Olovsson L., Livermore Software Technology Corp.

On Airbag Simulation in LS-DYNA with the Use of the Arbitrary Eulerian Method

Fokin D., Fredriksson L., Lokhande N., Altair GmbH

FTSS Dummy Model Updates

Huang Y., First Technology Safety Systems

Application of MADYMO Occupant Models in LS-DYNA/MADYMO Coupling

Happee R., Janssen A.J., Fraterman E., Monster J.W., TNO Automotive

FAT Dummy Models for Side Impact

Franz U., Schuster P., Schmid W., DYNAmore GmbH

Crash Simulation in Pedestrian Protection

Dörr S., Chladek H., IHF

Biomechanical Analysis of Whiplash Injuries; Women are not Scaled Down Men

Mordaka J., Gentle C. R., Univ. of Nottingham

Material Modelling

The Application of the Damage and Fracture Material Model to Crashworthiness Evaluations for Aluminum cars

Tsuchida T., Toyota Motor Corp.

Application of Configurational Forces in Finite Element Simulations

Kolling S., Ackermann D., DaimlerChrysler AG

A Simplified Approach for the Simulation of Rubber under Dynamic Loading

Du Bois P., Consultant

Improved Plasticity and Failure Models for Extruded Mg-Profiles in Crash Simulations

Oberhofer G., MATFEM; Lanzerath H., Wesemann J., Ford Research Center

Homborgsmeier E., EADS Corporate Research Center

Strain Rate Dependent Micro-mechanics Based Composite Material Model

Tabiei A., Ivanov I., University of Cincinnati

Implementation and Validation of the J-H2 Ceramic Material Model in LS-DYNA

Cronin D. S., Bui K., Berstad T., Kaufmann C., McIntosh G., University of Waterloo

On Constitutive Equations for Elastomers and Elastomeric Foams

Feng W.W., Hallquist J.O., Livermore Software Technology Corp.

Implementation of a Material Model for TRIP Steels in LS-DYNA and Comparison with Test Results

Hilding D., Engineering Research Nordic AB; Scheduling E., Avesta Polaroid AB

Maritime / Aerospace (Fluid-Structure Interaction)

LS-DYNA Applications in Shipbuilding

Le Sourne H., Besnier F., Couty N., Principa Marine ; Legarve H., DCN Ingénierie

Jet Engine Fan Blade Containment using Two Alternate Geometries

Carney K., Pereira M., Revilok D., NASA Res. Center; Matheny P., Florida Turbine Technology

Hydrodynamic Ram Analysis of Non-Exploding Projectile Impacting Water

Poehlmann-Martins F., Gabrys J., The Boeing Company; Souli M., University of Lille

The Dynamical Behaviors Analysis of Power Transmission Line with Wind Consideration

Nguyen T. L., Korea Maritim University

The Use of LS-DYNA Fluid-Structure Interaction to Simulate Fluid-Driven Deformation in the Aortic Valve

Carmody C.J., MG Bennett & Associates Ltd; Burriesci G., Sorin Biomedica Cardio; Howard I.C., Patterson E.A., University of Sheffield

ALE and Fluid Structure Interaction in LS-DYNA

Souli M., University of Lille; Olovsson L., Livermore Software Technology Corp

Metal Forming

Application of Dynamic Explicit in the Simulation of Superplastic Forming

Samekto H., University of Stuttgart; Roll K., DaimlerChrysler AG

New Developments at the forming Simulation of Hydroforming Processes

Keigler M., Hall R., Mihsein M., Bauer H., Aalen University of Applied Science

Influence of the Effect of Strain Rates on Springback in Aluminium 2024

Kulkarni P., Cessna Aircraft Company

Finite Element Analysis of Contact Stresses Due to Spherical Contact Conditions on an Elastic Surface

Ram A., Danckert J., Faurholdt T., Aalborg University; Rietz H., Danish Technological Institute

Virtual Die Tryout of Miniature Stamping Parts

Yang M.-C., Tsai T.-C., Metal Industries R&D Center

Sheet Metal Forming in a Virtual Reality Environment using LS-DYNA and Neural Networks

Gokhale A., Wichita State University

More Realistic Virtual Prototypes by Means of Process Chain Optimization

Gantner P., Harrison D.K., DeSilva A.K.M., Bauer H., Aalen University of Applied Science

New Trends in Sheet Metal Forming

Buchert J., Harrison D.K., DeSilva A.K.M., Bauer H., Aalen University of Applied Science

Stress Analysis of Connector PIN Produced by Reverse Stamping Process

Won Y.-H., LG-Cable Ltd.

Simulation of the Forming Process of Metal-Plastic-Metal Sheets

Borg R., Engineering Research Nordic AB

Optimization

Shape Adaptive Airfoils for Turbomachinery Applications: Simulation and Optimization

Müller T., Lawrenz M., University of Kassel

Stochastic Optimization in LS-OPT

Stander N., Roux W.J., Livermore Software Techn. Corp; Giger M., Redhe M., Linköping University

System Identification and Design Optimization of "Noisy" Structural Problems: Probabilistic and Deterministic Fundamentals

Stander N., Roux W.J., Livermore Software Techn. Corp.

Geometry Optimization using Stochastic Methods

Höfer C., Sakaryali C., EASi Engineering GmbH

Optimization of a Cockpit Structure according to ECE-R 21 Regulation

Walter M., Chladek H., IHF

A Method for Modifying the Forming Tool Geometry in Order to Compensate for Springback Effects

Jernberg A., Engineering Research AB

New Developments / Theory

Recent Developments in LS-DYNA

Hallquist J.O., Livermore Software Technology Corp.

Theory of Contact Algorithms

Wriggers P., University of Hannover

Using LS-Dyna for Heat Transfer

Shapiro A., Livermore Software Technology Corporation

Stabilized DSG Elements - A New Paradigm in Finite Element Technology

Bischoff M., Koschnick F., Bletzinger K.-U., Univ. Munich

Implicit Analysis using LS-DYNA

Grimes R., Livermore Software Technology Corp.

Simulation of Full-Scale Seismic-Resistant Structural Frame Tests Using LS-DYNA 960 Implicit Solver

Walker B., ARUP; Fielding C.J., Ove Arup & Partners California Ltd.

Examples Manual for *User_Loading Option

Adoum M., Lapoujade V., CRIL Technology

LS-DYNA Beam Element Cross Section Interaction - An Assessment

Schwer L., Schwer Engineering & Consulting Services

Drop Test / Impact

Structural Design Review of LCD-TV Module by Impact Analysis

Choi S., Lee J.-G., Samsung Electronics Co.

The Relation between Initial Yaw and Long Rod Projectile Shape After Penetration an Oblique Thin Plate

Arad M., Tuati D., Latovitz I., Israel Military Industries

Simulation of a Drop onto a Punch of a Transport Container for Nuclear Fuel Assemblies

Marchaud G., Werle J., Cogema Logistics

Drop Test Simulation of a Transport Container for Highly Active Nuclear Waste

Werle J., Marchaud G., Cogema Logistics

Numerical Simulation of a Flight Recorder's; Protective Case Penetration Resistance Test

Ryabov A., Romanov V., Kukanov S., Roschihmarov D., Sarov Open Computing Center

Numerical Modelling of Impacts on Ski Safety Nets

Adoum M., Lapoujade V., CRIL Technology

Impact on Textiles

Schweizerhof K., DYNAmore GmbH; Finckh H., ITV Denkendorf

MPP / Linux-Cluster / Hardware Performance

LS-DYNA on MPP Platforms, Experience and Practical Recommendations

Jankowski U., Tecosim GmbH

LS-DYNA on Linux-Cluster at EDAG - Use Case

Hanlon J., EDAG Engineering+Design AG

Performance of LS-DYNA on Intel Itanium; 2 Processor-Based Clusters

Chaltas G., Prince T., Margo W., Jonsson L., Intel Corp.

The New Paradigm Shift for High-Performance Computing

Cornelius H., Intel GmbH

Considerations for LS-DYNA Efficiency in the SGI IRIX and Linux Environments with a NUMA System Architecture

Posey S., Meng N., Silicon Graphics

Performance of LS-DYNA on hpcLine Linux Clusters

Altmeyer K., Fujitsu Siemens Computers GmbH

Linux Cluster - Computer Power Out of the Box

Gaier K., science+computing ag

A Correlation Study between MPP LS-DYNA Performance and Various Interconnection Networks

Lin Y.-Y., Hewlett-Packard Ltd.

Itanium - A Viable Cost-Effective Technology for Crash Simulation

Hillcoat A., Hewlett-Packard Ltd.

Recent Developments of LS-DYNA Computation in Sun Microsystems

Roh Y.-S., Fong H., Sun Microsystems Inc.

LS-DYNA Environment

CAE Data Management and Quality Assessment of LS-DYNA Crash Models using V-CESS

Eick M., Seybold J., Fredriksson L., Altair GmbH

Automating LS-DYNA Simulation Processes using SOFY/RADE

Ulrich D., Sofy GmbH

scFEMod - The New Preprocessor for Efficient Assembly and Model Validation

Gaier K., science+computing ag

Platform and LS-DYNA, solutions for design & simulation - today and tomorrow

Slominsky M., Reichert C., Platform Computing GmbH

Automatic Assembly of a Full Car Crash Model using MEDINA 7.2

Aldinger V., T-Systems

Advanced Services on hpcPortal - Usage of MIDAS for Crash Simulation on Linux Clusters

Sattler M., Finkel A., T-Systems

Registration and contact address

DYNAMore GmbH, Mrs. Kathleen Ryssel

Industriestr. 2 • D-70565 Stuttgart • Germany

Phone: +49 (0)711 - 459600 - 0 - Fax: +49 (0)711 - 459600 - 29

E-mail: info@dynamore.de, <http://www.dynamore.de>

Conference web site:

<http://www.ls-dynaconferences.de>

Special Announcements and Highlights of News Pages

Posted on FEA Information in January - Archived on the news page

January 06	Fujitsu PRIMEPOWER
	AMD Athlon™ MP Processor for Servers
	State Unitary Enterprise – STRELA – Distributor in Russia
January 13	ANSYS Inc.'s AI*Solutions
	LSTC's LS-OPT
	Flotrend – Distributor in Taiwan
January 20	MSC.visualNastran 4D™
	JRI Professional Engineering
	Theme Engineering – Distributor in Korea
January 27	SGI – “Scaling Linux to New Altitudes”
	Oasys and Arup
	DYNAmore – Distributor in Germany

February Featured Publication * - Archived on the publication page

****Shape Optimization of Crashworthiness Structures - Dave J. Eby, applied Computational Design Associates, Inc.***

Improving Crash Analysis Through The Estimation of Residual Strains Brought About by Forming Metal - William Broene, Brown Corporation

Study on Optimal Design of Automotive Body Structure Crashworthiness - Hailang Wang, Shanghai Jiao Tong University

Special Announcement: **Corrado Tumminelli, Numerica Srl - Italy**
Ph +39.055.432010 www.numerica-srl.it
c.tumminelli@numerica-srl.it

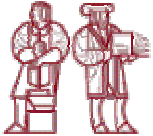
2003 March 13-14: Training on "Pedestrian Safety, design strategies and tools for the pedestrian safety under EEVC (European) rules". The LS-DYNA simulation of vehicle impact on pedestrians is discussed, with the aim to design a cars front end in a way that decreases injury to the impacted pedestrian. For details: c.tumminelli@numerica-srl.it

2003 March 18: Seminar on "VPS - Virtual Paint Shop" Car painting and drying processes simulation are introduced. From the EDC (electro deposition coating) painting, to the DIP (simulation of the body immersion with regard to the paint stagnation into the body cavities), to the oven drying process, the computer simulations deliver huge savings in time and cost. All the major European car makers are starting to use this virtual approach. Implicit code is used.

FEA Information Participants

Headquarters	Company	
Australia	Leading Engineering Analysis Providers	www.leapaust.com.au
Canada	Metal Forming Analysis Corp.	www.mfac.com
France	Cril Technology Simulation	www.criltechnology.com
Germany	DYNAmore	www.dynamore.de
Germany	CAD-FEM	www.cadfem.de
India	GissEta	www.gisseta.com
Italy	Altair Engineering srl	www.altairtorino.it
Italy	Numerica srl	www.numerica-srl.it
Japan	The Japan Research Institute, Ltd	www.jri.co.jp
Japan	Fujitsu Ltd.	www.fujitsu.com
Korea	THEME Engineering	www.lsdyna.co.kr
Korea	Korean Simulation Technologies	www.kostech.co.kr
Russia	State Unitary Enterprise - STRELA	www.ls-dynarussia.com
Sweden	Engineering Research AB	www.erab.se
Taiwan	Flotrend Corporation	www.flotrend.com
UK	OASYS, Ltd	www.arup.com/dyna
USA	INTEL	www.intel.com
USA	Livermore Software Technology	www.lstc.com
USA	Engineering Technology Associates	www.eta.com
USA	ANSYS, Inc	www.ansys.com
USA	Hewlett Packard	www.hp.com
USA	SGI	www.sgi.com
USA	MSC.Software	www.mssoftware.com
USA	DYNAMAX	www.dynamax-inc.com
USA	CEI	www.ceintl.com
USA	AMD	www.amd.com
USA	Dr. T. Belytschko	Northwestern University
USA	Dr. D. Benson	Univ. California – San Diego
USA	Dr. Bhavin V. Mehta	Ohio University
USA	Dr. Taylan Altan	The Ohio State U – ERC/NSM
USA	Prof. Ala Tabiei	University of Cincinnati
Russia	Dr. Alexey I. Borovkov	St. Petersburg State Tech. University
Italy	Prof. Gennaro Monacelli	Prode – Elasis & Univ. of Napoli, Federico II

EVENTS – CONFERENCES – EXPO’s

2003	
March 18-19	Russian Automotive Conference , Moscow, Russia
May 19-21 	BETECH 2003 taking place at the Hyatt Regency Dearborn hotel in Detroit, USA - 15th International Conference on Boundary Element Technology
May 22 - 23	4th European LS-DYNA Conference will be held in ULM, Germany
June 3-5	Testing Expo 2003 , Stuttgart, Germany.
June 17-20 	The Second M.I.T. Conference on Computational Fluid and Solid Mechanics , taking place at Massachusetts Institute of Technology Cambridge, MA.,USA
Oct 29-31	Testing Expo North America 2003 - located Novi Expo Center in Detroit, Michigan.
Nov 12-14	CAD-FEM User Conference 2003 - Dorint Sanssouci Hotel, Berlin Potsdam.

If you have an event you would like posted send it to mv@feainformation.com

Zero Energy Modes in One Dimension: An Introduction to “Hourglass” Modes

David J. Benson

January 20, 2003

Reduced integration does a lot of good things for an element: it reduces the computational cost, it reduces shear and volume locking, and it generally softens the element so that the predicted stress is more accurate. However, reduced integration also makes elements too soft in the sense that modes other than rigid body modes aren't resisted by the element. These modes, which were originally noticed in finite difference calculations in two dimensions in the 1960s, are historically called *hourglass* or *keystone* modes because of their shape. For other elements, the modes don't have these shapes, and the modes are commonly referred to as *zero energy* modes.

1 Mathematical Preliminaries: Vectors and Covectors

When we are working in cartesian space, such as (x_1, x_2) with the basis vectors \mathbf{e}_1 and \mathbf{e}_2 , an arbitrary vector in the space, \mathbf{a} , can be written

$$\mathbf{a} = (\mathbf{a} \cdot \mathbf{e}_1)\mathbf{e}_1 + (\mathbf{a} \cdot \mathbf{e}_2)\mathbf{e}_2 = a_1\mathbf{e}_1 + a_2\mathbf{e}_2. \quad (1)$$

Suppose, however, that two other basis vectors, $\hat{\mathbf{e}}_1$ and $\hat{\mathbf{e}}_2$, are chosen and they aren't perpendicular to each other and, just to make things a little more complicated, they don't have a unit length. Expressing \mathbf{a} in terms of these new basis vectors isn't as simple as it was for \mathbf{e}_1 and \mathbf{e}_2 . Our goal is to determine the coefficients \hat{a}_1 and \hat{a}_2 so that

$$\mathbf{a} = \hat{a}_1\hat{\mathbf{e}}_1 + \hat{a}_2\hat{\mathbf{e}}_2. \quad (2)$$

The most direct approach is to solve two linear equations for the coefficients which are generated by taking the dot product of Equation 2 with \mathbf{e}_1 and \mathbf{e}_2 , namely

$$\begin{bmatrix} \hat{\mathbf{e}}_1 \cdot \mathbf{e}_1 & \hat{\mathbf{e}}_2 \cdot \mathbf{e}_1 \\ \hat{\mathbf{e}}_1 \cdot \mathbf{e}_2 & \hat{\mathbf{e}}_2 \cdot \mathbf{e}_2 \end{bmatrix} \begin{Bmatrix} \hat{a}_1 \\ \hat{a}_2 \end{Bmatrix} = \begin{Bmatrix} a_1 \\ a_2 \end{Bmatrix}. \quad (3)$$

The solution is

$$\frac{1}{\det} \begin{bmatrix} \hat{\mathbf{e}}_2 \cdot \mathbf{e}_2 & -\hat{\mathbf{e}}_2 \cdot \mathbf{e}_1 \\ -\hat{\mathbf{e}}_1 \cdot \mathbf{e}_2 & \hat{\mathbf{e}}_1 \cdot \mathbf{e}_1 \end{bmatrix} \begin{Bmatrix} a_1 \\ a_2 \end{Bmatrix} = \begin{Bmatrix} \hat{a}_1 \\ \hat{a}_2 \end{Bmatrix}. \quad (4)$$

The solution can be re-written in the form of a vector dot product if we define the vectors $\hat{\mathbf{E}}_1$ and $\hat{\mathbf{E}}_2$ as

$$\hat{\mathbf{E}}_1 = \frac{1}{\det} \begin{Bmatrix} \hat{\mathbf{e}}_2 \cdot \mathbf{e}_2 \\ -\hat{\mathbf{e}}_2 \cdot \mathbf{e}_1 \end{Bmatrix} \quad \hat{\mathbf{E}}_2 = \frac{1}{\det} \begin{Bmatrix} -\hat{\mathbf{e}}_1 \cdot \mathbf{e}_2 \\ \hat{\mathbf{e}}_1 \cdot \mathbf{e}_1 \end{Bmatrix} \quad (5)$$

$$\hat{a}_1 = \mathbf{a} \cdot \hat{\mathbf{E}}_1 \quad \hat{a}_2 = \mathbf{a} \cdot \hat{\mathbf{E}}_2. \quad (6)$$

These special vectors are the *covectors* for $\hat{\mathbf{e}}_1$ and $\hat{\mathbf{e}}_2$. Some properties are fairly obvious: the covectors of the covectors are the original set of basis vectors, and that for a Cartesian coordinate system, the basis vectors are their own covectors. It is, however, important to remember that basis vectors and covectors both come in sets: the covector $\hat{\mathbf{E}}_1$ is not just a function of $\hat{\mathbf{e}}_1$, but also of all the other basis vectors. Change the other basis vectors, and $\hat{\mathbf{E}}_1$ will also change even if $\hat{\mathbf{e}}_1$ remains unchanged. The vectors and their covectors have the property

$$\hat{\mathbf{E}}_i \hat{\mathbf{e}}_j = \delta_{ij} \quad (7)$$

but, in general,

$$\hat{\mathbf{E}}_i \hat{\mathbf{E}}_j \neq \delta_{ij} \quad \hat{\mathbf{e}}_i \hat{\mathbf{e}}_j \neq \delta_{ij}. \quad (8)$$

To make these ideas a little more concrete, let's consider an example in two dimensions, with the basis vectors $\hat{\mathbf{e}}_1 = \{1 \ 0\}^T$ and $\hat{\mathbf{e}}_2 = \{\cos(\theta) \ \sin(\theta)\}^T$. The system of equations to be solved for \hat{a}_1 and \hat{a}_2 is

$$\begin{bmatrix} 1 & \cos(\theta) \\ 0 & \sin(\theta) \end{bmatrix} \begin{Bmatrix} \hat{a}_1 \\ \hat{a}_2 \end{Bmatrix} = \begin{Bmatrix} a_1 \\ a_2 \end{Bmatrix}. \quad (9)$$

Solving the system gives

$$\frac{1}{\sin(\theta)} \begin{bmatrix} \sin(\theta) & -\cos(\theta) \\ 0 & 1 \end{bmatrix} \begin{Bmatrix} a_1 \\ a_2 \end{Bmatrix} = \begin{Bmatrix} \hat{a}_1 \\ \hat{a}_2 \end{Bmatrix} \quad (10)$$

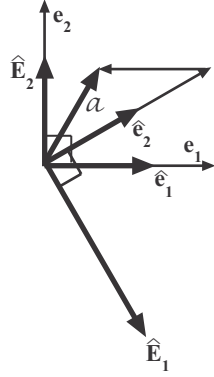


Figure 1: The vectors and covectors for θ equals 30 degrees.

and the covectors are therefore (see Figure 1)

$$\hat{\mathbf{E}}_1 = \left\{ \begin{array}{c} 1 \\ -\frac{\cos(\theta)}{\sin(\theta)} \end{array} \right\} \quad \hat{\mathbf{E}}_2 = \left\{ \begin{array}{c} 0 \\ \frac{1}{\sin(\theta)} \end{array} \right\}. \quad (11)$$

The reason for introducing vectors and covectors here is \mathbf{B} can be thought of as being a collection of covectors corresponding to the nodal displacements associated with the different strain modes of an element. For example, in two dimensions $\epsilon_{11} = \partial u_1 / \partial x_1$, and therefore a set of nodal displacements having the form $\{x_1, 0, x_2, 0, \dots, x_n, 0\}$, when multiplied by the first row of \mathbf{B} will give the result $\epsilon_{11} = 1$. If this displacement vector is labelled \mathbf{b}_1 , its covector is \mathbf{B}_1 , the first row in \mathbf{B} . An arbitrary displacement vector for an element could therefore be expressed as

$$\mathbf{d} = (\mathbf{B}_1 \cdot \mathbf{d}) \mathbf{b}_1 \dots = \epsilon_{11} \mathbf{b}_1 \dots \quad (12)$$

Since an element has more degrees of freedom than it has strains, the displacement modes must be expanded to include other modes (e.g., rigid body modes) to form a complete basis for the displacements of the nodes of the element.

A particular type of mode that shows up in under-integrated elements is the zero energy mode. The mathematics of vectors and covectors gives us a language to use for discussing these zero energy modes, and the corresponding extra rows of \mathbf{B} required to calculate their amplitude.

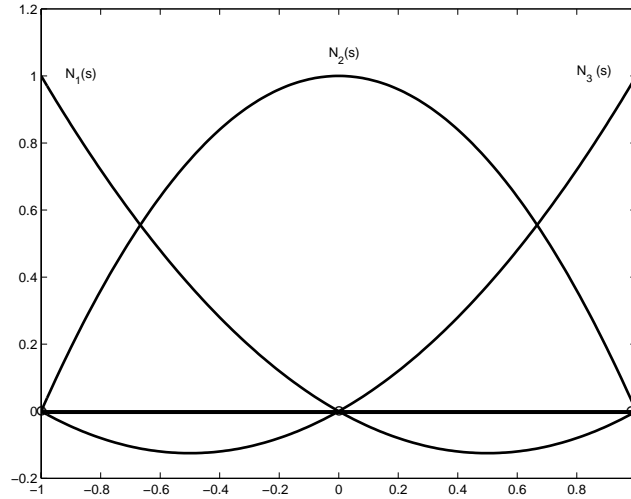


Figure 2: The shape functions for a one-dimensional quadratic element.

2 Zero Energy Modes in One Dimension

All the basic concepts associated with zero energy modes are easily demonstrated in one dimension with a three-node quadratic element using one-point integration. The interpolation functions and their derivatives for the three nodes (see Figure 2) are

$$N_1(s) = \frac{1}{2}s(s-1) \quad (13)$$

$$N_2(s) = 1 - s^2 \quad (14)$$

$$N_3(s) = \frac{1}{2}s(s+1) \quad (15)$$

$$\frac{\partial N_1}{\partial s} = s - \frac{1}{2} \quad (16)$$

$$\frac{\partial N_2}{\partial s} = -2s \quad (17)$$

$$\frac{\partial N_3}{\partial s} = s + \frac{1}{2} \quad (18)$$

The \mathbf{B} matrix, for a general location within the element, is therefore

$$\mathbf{B}(s) = \frac{1}{\det(J)} \begin{bmatrix} s - \frac{1}{2} & -2s & s + \frac{1}{2} \end{bmatrix} \quad (19)$$

$$J = x_1(s - \frac{1}{2}) + x_2(-2s) + x_3(s + \frac{1}{2}) \quad (20)$$

The nodal displacement vector corresponding to a uniform strain of 1 is $\{ x_1 + c \ x_2 + c \ x_3 + c \}^T$, where c is any arbitrary constant, and corresponds to a rigid body translation of c . For convenience, we'll call this displacement vector \mathbf{b} .

A second nodal displacement vector is the rigid body translation

$$\mathbf{r} = \{ 1 \ 1 \ 1 \}^T \quad (21)$$

and its corresponding covector is

$$\mathbf{R} = \{ 1/3 \ 1/3 \ 1/3 \}^T. \quad (22)$$

The product $\mathbf{B} \cdot \mathbf{r} = 0$, but $\mathbf{R} \cdot \mathbf{b} = 1/3(x_1 + x_2 + x_3) + c$. To make $\mathbf{R} \cdot \mathbf{b} = 0$, we set $c = -1/3(x_1 + x_2 + x_3)$. This is strictly for convenience since only linear independence is required.

Since the element has three nodes, the vector space of its nodal displacements has a dimension of three and is spanned by any three linearly independent vectors. This implies that there is a third vector that is linearly independent of \mathbf{b} and \mathbf{r} that can be used to complete the space. Furthermore, there is a covector corresponding to this third vector which completes the covector space for the element.

One choice for the third displacement vector becomes apparent when the element is integrated using one-point integration, where the location and weight are $s = 0$ and $w = 2$, respectively. The strain displacement matrix \mathbf{B} simplifies to

$$\mathbf{B} = \frac{1}{L} \begin{bmatrix} -1 & 0 & 1 \end{bmatrix}. \quad (23)$$

$$L = x_3 - x_1 \quad (24)$$

The strain in the element is therefore not a function of the displacement at node 2, and if nodes 1 and 3 don't move, the element won't generate any stress regardless of the displacement of node 2. In a similar manner, since the force vector is $\mathbf{B}^T \sigma(x_3 - x_1)$, node 2 won't experience any force due to the stress in the element.

By inspection, this peculiar mode, which we'll label \mathbf{h} , is

$$\mathbf{h} = \{ 0 \ 1 \ 0 \}^T \quad (25)$$

and it is orthogonal to $\mathbf{B}(0)$, i.e., $\mathbf{B}(0) \cdot \mathbf{h} = 0$. The element stiffness matrix for one-point integration is

$$\mathbf{K} = EL\mathbf{B} \otimes \mathbf{B}, \quad (26)$$

and therefore the strain energy associated with this mode is

$$U = \frac{1}{2} \mathbf{h}^T \mathbf{K} \mathbf{h} = 0. \quad (27)$$

The mode \mathbf{h} is therefore a *zero energy* mode.

If a calculation is performed using this element, numerical roundoff errors in explicit calculations will possibly lead to the motions of the central nodes of the elements being the ones with the largest amplitudes in the calculation. Since these zero energy modes are orthogonal to the stress and strain in the elements, they don't affect the accuracy of the remainder of the solution. In implicit quasi-static calculations, the rows and columns associated with the middle nodes are zero, and the stiffness matrix is singular. In multi-dimensional calculations, the zero energy modes may cause negative Jacobians in the elements, which ends the analysis. A means of reducing the impact of the zero energy modes on the calculation is therefore desirable.

Hourglass modes may be controlled by adding either stiffness or viscosity terms to the equations. In large deformation calculations, a viscous term is usually preferred to avoid building up large elastic forces in the system. Stiffness terms are used in implicit quasi-static calculations to eliminate the singularity of the stiffness matrix. For explicit calculations with small to moderate deformations, and long time periods, a stiffness form of hourglass control is often preferred to prevent hourglass modes from slowly building up in the solution. Combinations of viscous and stiffness hourglass control are also sometimes used, but usually one form of the control is adequate for most calculations.

The simplest formulation to control the zero energy modes, which was used originally in the finite difference community, is to simply add a viscous term to the element force calculations,

$$\mathbf{F} = \mathbf{B}^T \sigma L + cL\mathbf{h} \otimes \mathbf{h}\dot{u} \quad (28)$$

where c is a small damping coefficient. In a similar manner, the finite element community added a term to the stiffness matrix,

$$\mathbf{K} = EL\mathbf{B} \otimes \mathbf{B} + eL\mathbf{h} \otimes \mathbf{h} \quad (29)$$

where e is a small elastic constant.

There is, however, one unfortunate problem with this simple formulation, and that is the zero energy mode \mathbf{h} isn't orthogonal to the rigid body mode \mathbf{r} . The zero energy mode control in Equations 28 and 29 will resist rigid body motion, a highly undesirable, nonphysical response. The appropriate vector to use is the covector \mathbf{H} . Just as \mathbf{B} is orthogonal to \mathbf{r} and \mathbf{h} , and \mathbf{R} is orthogonal to \mathbf{b} and \mathbf{h} , \mathbf{H} needs to be orthogonal to \mathbf{b} and \mathbf{r} . The required covector is generated using Graham-Schmidt orthogonalization, a procedure for making vectors orthogonal to each other, with \mathbf{h} as the initial "guess" for \mathbf{H} ,

$$\mathbf{H} = \mathbf{h} - (\mathbf{h} \cdot \mathbf{R})\mathbf{r} \quad (30)$$

$$= [-1/3 \quad 2/3 \quad -1/3]^T. \quad (31)$$

Substituting \mathbf{H} for \mathbf{h} in Equations 28 and 29 gives two formulations for controlling the hourglass mode without opposing rigid body motion or altering the constant strain response,

$$\mathbf{F} = -\mathbf{B}^T \sigma L - cL\mathbf{H} \otimes \mathbf{H} \dot{\mathbf{u}} \quad (32)$$

$$\mathbf{K} = EL\mathbf{B} \otimes \mathbf{B} + eL\mathbf{H} \otimes \mathbf{H} \quad (33)$$

Summarizing our results so far, the quadratic element has three basic displacement modes:

1. The rigid body translation mode $\mathbf{r} = \{ 1 \quad 1 \quad 1 \}^T$.
2. The strain mode $\mathbf{b} = \{ -L/2 \quad 0 \quad L/2 \}^T$. This mode has been normalized so that $\mathbf{B} \cdot \mathbf{b} = 1$.
3. The zero energy mode $\mathbf{h} = \{ -1/2 \quad 1 \quad -1/2 \}^T$, which has been normalized so that $\mathbf{H} \cdot \mathbf{h} = 1$ and it has been orthogonalized with respect to \mathbf{r} and \mathbf{b} .

Since the element only has three degrees of freedom, and the three modes are linearly dependent, these modes span the entire space of possible deformations for the element.

Corresponding to the three displacement modes are the three covectors that detect the amplitudes of the displacement modes in an arbitrary displacement vector:

1. $\mathbf{R} = [1/3 \ 1/3 \ 1/3]$ is the rigid body covector.
2. $\mathbf{B} = [-1/L \ 0 \ 1/L]$ is the familiar strain-displacement matrix.
3. $\mathbf{H} = [-1/3 \ 2/3 \ -1/3]$.

Just as the three displacement modes span the element's vector space, the covectors span its covector space. For example, the general form for the strain-displacement matrix, $\mathbf{B}(s)$ can be expressed in terms of the covectors as

$$\mathbf{B}(s) = \frac{L}{2\det(J)}\mathbf{B} - \frac{3s}{\det(J)}\mathbf{H}. \quad (34)$$

The element stiffness matrix, for uniformly spaced nodes, with exact integration is

$$\mathbf{K} = \int_{-1}^{+1} E\mathbf{B}^T(s)\mathbf{B}(s)\det(J)ds \quad (35)$$

$$= \frac{E}{L} \begin{bmatrix} 7/3 & -8/3 & 1/3 \\ -8/3 & 16/3 & -8/3 \\ 1/3 & -8/3 & 7/3 \end{bmatrix} \quad (36)$$

Substituting Equation 34 into Equation 35 results in three terms,

$$\mathbf{K} = \int_{-1}^{+1} E\frac{L^2}{4\det^2(J)}\mathbf{B}^T\mathbf{B}\det(J)ds \quad (37)$$

$$- \int_{-1}^{+1} E\frac{3Ls}{\det^2(J)}(\mathbf{B}^T\mathbf{H} + \mathbf{H}^T\mathbf{B})\det(J)ds \quad (38)$$

$$+ \int_{-1}^{+1} E\frac{9s^2}{\det^2(J)}\mathbf{H}^T\mathbf{H}\det(J)ds. \quad (39)$$

The first integral is the stiffness matrix that is obtained using 1-point integration. The second term, which is zero because $\int s ds = 0$, doesn't contribute to either the exact stiffness or numerically integrated stiffness matrices. The third term is the difference between the exactly integrated stiffness matrix and the one-point integration. Choosing

$$eL = \int_{-1}^{+1} E\frac{9s^2}{\det(J)}ds = \frac{12E}{L} \quad (40)$$

for Equation 33 gives the exact stiffness matrix (for equally spaced nodes) with one-point integration. This approach is also applicable to elements in two and three dimensions.

3 Implementation in an Explicit Code

The implementation of the viscous and stiffness forms of the zero energy mode control in an explicit finite element code are very similar. Calculating the matrix $\mathbf{H} \otimes \mathbf{H}$ requires n^2 floating point multiplies for an element with n degrees of freedom. The cost of a matrix-vector multiply $\mathbf{H} \otimes \mathbf{H}\mathbf{u}$ is also high, requiring $2n^2 - n$ floating point operations. The implementation of the zero energy mode control is therefore structured to avoid matrix operations.

For the current discussion, we'll assume that both viscous and stiffness control is used and that it has the form

$$\mathbf{F} = -e\mathbf{H} \otimes \mathbf{H}\mathbf{u} - c\mathbf{H} \otimes \mathbf{H}\dot{\mathbf{u}}. \quad (41)$$

The original implementations assumed that e and c are constants, but more recent formulations have made them time dependent functions of the material model, which makes a rate form for the stiffness contribution necessary. The rate form is also attractive even if e is constant because many explicit codes don't routinely store the total displacement vector, \mathbf{u} . A generalized force, f_h , is stored for each element,

$$f_h(t) = \int_0^t e\mathbf{H} \cdot \mathbf{u} dt. \quad (42)$$

The resulting implementation evaluates, in sequence,

$$\dot{\alpha} = \mathbf{H} \cdot \dot{\mathbf{u}} \quad (43)$$

$$f_h^{n+1} = f_h^n + \Delta t e \dot{\alpha} \quad (44)$$

$$\mathbf{F} = (-f_h^{n+1} - c\dot{\alpha})\mathbf{H}. \quad (45)$$

The dot product for calculating $\dot{\alpha}$ requires $2n - 1$ floating point operations, the update of f_h^{n+1} requires 3, and the final evaluation of the force requires $n + 2$, for a total of $3n + 4$ operations. This implementation is therefore approximately n times faster than evaluating $\mathbf{H} \otimes \mathbf{H}$ and performing the matrix multiply. For an element with 3 degrees of freedom, this cost ratio isn't terribly important, but for an 8-node brick element, which has 24 degrees of freedom, the difference in cost is substantial.